# Structural Integrity Analysis of Lightweight Alloys for Aerospace Applications


## Manuscript Info

***Manuscript History***
Received: xxxxxxxxxxxxxxx
Final Accepted: xxxxxxxxxxx
Published: xxxxxxxxxxxxxxx

***Key words:-***
Lightweight Alloys, HPT Blade, FEA, Nickle-based Superalloys



## Abstract

In the present investigation, a structural integrity analysis of an HPT blade made of three state-of-the-art nickel-based single-crystal superalloys, namely, CMSX-4, CMSX-8, and CMSX-4 Plus, is discussed. The finite element method (FEM) analysis has been performed for analysing the distribution of stresses, strain, deformation, and the factor of safety under practical mechanical and thermal loads that occur under the aero-engine environment. The geometry of the blade was modelled with critical aerodynamic characteristics, meshed using detailed tetrahedral elements, and exposed to suitable boundary conditions such as fixed support at the root and constant surface pressure. Material properties for every alloy were inputted according to experimentally confirmed data. The outcome indicated similar maximum equivalent stresses for all materials but displayed variation in strain, deformation, and safety margins. CMSX-8 had the lowest deformation and strain and the highest factor of safety, which means better mechanical performance than CMSX-4 and CMSX-4 Plus. The results agree that the selection of material strongly affects the HPT blade's durability and performance. CMSX-8 turned out to be the strongest of the materials researched and thus became the best bet for future applications as high-performance turbine blades.






## Introduction: -

High-pressure turbine (HPT) blades are key elements in advanced jet engines, which are subjected to harsh conditions of high temperatures, large mechanical stresses, and corrosive atmospheres. Such severe conditions require materials that can sustain structural integrity, creep deformation resistance, and oxidation resistance during long service life. The drive for higher engine efficiencies and lower emissions has further accelerated the research and development of advanced materials withstanding such extreme operating conditions.

Nickel-based single-crystal superalloys are becoming the preferred material for HPT blades owing to their improved high-temperature strength, creep, and corrosion resistance. Amongst these, CMSX-4, CMSX-8, and CMSX-4 Plus have been comprehensively evaluated and used. CMSX-4, which belongs to the second generation of superalloys, provides an ideal balance between the mechanical characteristics and ease of production. CMSX-8, a third-generation alloy, has rhenium added for greater creep resistance. CMSX-4 Plus is a development of CMSX-4 made for delivering enhanced phase stability and performance at high temperatures [1].

Recent studies have explored different facets of these superalloys. For example, investigations have examined the influence of laser shock peening on CMSX-4's microstructure and mechanical properties, which exhibited surface hardness and crack initiation resistance improvement [2]. Other publications have also explored the stress corrosion behavior of CMSX-4 and its performance in corrosive conditions [3]. Life prediction models for CMSX-4 turbine blades have been established, considering thermo-mechanical loads and fatigue-creep interactions, which are essential for improving blade durability [4]. Moreover, new repair methods, including high-velocity air fuel (HVAF) spraying, have been investigated to recover the integrity of CMSX-4 components following operational damage [5].

## Material

### Development and Composition of CMSX Superalloys

The ever-increasing need for greater efficiency and performance in jet engines has spurred the development of nickel-based single-crystal superalloys, particularly the CMSX series. CMSX-4, which was developed as a second-generation alloy, has about 3% rhenium and provides a balanced combination of creep resistance and

workability [1]. CMSX-8 is the third generation of such alloys with increased rhenium content and balanced alloying additions like tungsten and tantalum to enhance high-temperature strength and phase stability further [6]. At the same time, CMSX-4 Plus was designed to improve the initial CMSX-4 by minimizing the γ/γ′ lattice mismatch and enhancing phase stability for long-term exposures above 1100 °C [7].

Alloying schemes, especially regulation of the fraction of the γ′ phase and reduction of undesirable phases like TCP phases, have been crucial to the success of these alloys [8]. Contemporary computational thermodynamics methods such as CALPHAD have facilitated improved prediction of phase stability and optimization of trace alloying elements to optimize CMSX-4 Plus for advanced turbine applications.

**Microstructural Characteristics and Evolution during Service**

The enhanced mechanical behavior of CMSX-4, CMSX-8, and CMSX-4 Plus can be attributed significantly to their controlled microstructure dominated by the ordered γ′ ($Ni_3Al$) phase distributed uniformly in the γ matrix. The γ′ phase is the major strengthening agent, offering high-temperature dislocation motion resistance [9].

Experiments on CMSX-4 have revealed that heat treatment conditions play a decisive role in determining precipitate size, distribution, and morphology of the γ′ precipitates, thus having direct implications on mechanical properties [10]. Elevated temperature thermal aging or long-term service exposure causes coarsening of the γ′ phase and, under certain conditions, the nucleation of undesirable TCP phases, particularly in the more rhenium-contained alloys such as CMSX-8 [8].

Sophisticated characterization methods, including high-resolution transmission electron microscopy (HR-TEM) and atom probe tomography (APT), have identified nanoscale segregation behavior in CMSX-4 and CMSX-8 that is essential for phase stability upon high-temperature exposure. In CMSX-4 Plus, the decreased lattice misfit between the γ and γ′ phases inhibit the nucleation of TCP phases, thereby prolonging the material's high-temperature service life [11].

In addition, research in creep deformation has indicated rafting of the γ′ phase takes place due to long-time exposure to temperature and stress and leads to directionally coarsened structures which either improve or impair mechanical properties based on crystal orientation and state of stress.

**Mechanical Properties of CMSX-4, CMSX-8, and CMSX-4 Plus**

High-pressure turbine blade mechanical performance is particularly sensitive to tensile strength, creep resistance, fatigue life, and fracture toughness of the material. CMSX-4 was initially developed to be reliable up to ~1100 °C with superior creep strength due to its high-volume fraction of γ′ (~70%) [12]. The development of CMSX-8, with increased rhenium and tantalum levels, provided additional creep rupture life and low-cycle fatigue strength improvement at high temperatures.

Recent research has characterized the room temperature and high-temperature tensile properties of CMSX-4 and CMSX-8 and found that CMSX-8 shows greater tensile yield stress and ultimate tensile strength at temperatures above 900 °C than CMSX-4 [13]. CMSX-4 Plus demonstrates improved mechanical stability under cyclic loading conditions because of fine microstructure and improved defect nucleation suppression during service.

Regarding fatigue behavior, the development of fatigue cracks at the γ/γ′ interfaces continue to be a major concern. Nevertheless, CMSX-8 exhibits retardation in crack initiation and reduced rates of propagation, particularly under thermomechanical fatigue testing conditions that reflect jet engine operational environments [14]. Concurrently, innovations in alloying concepts for CMSX-4 Plus have enabled improved mechanical property retention following extensive cyclic exposure.

The anisotropic behavior of single-crystal superalloys also significantly contributes to mechanical performance. Recent research emphasizes that [001]-oriented CMSX-4 and CMSX-8 samples yield maximum creep and tensile performance based on alignment with the main slip systems of nickel.

**Thermal Properties and High-Temperature Performance**

Thermal characteristics like thermal conductivity, thermal expansion coefficient, and oxidation resistance are essential for the stable operation of HPT blades. CMSX-4 has been reported to exhibit constant thermal conductivity over a broad temperature range, though minor decreases are noted above 1000 °C due to microstructural coarsening [15].

CMSX-8, on the other hand, has slightly reduced thermal conductivity but considerably improved oxidation resistance due to the optimization of chromium and aluminium contents that support the development of protective oxide scales [16]. Research has proven that the introduction of elements such as rhenium (Re) and ruthenium (Ru) in CMSX-8 slows diffusion processes, slowing down the rates of oxidation and thermal degradation over extended service.

CMSX-4 Plus improves on these areas even further by raising the γ′ solvus temperature, thus widening the operating temperature range above 1150 °C without early microstructural degradation [17]. Current research shows that CMSX-4 Plus exhibits better cyclic oxidation resistance than both CMSX-4 and CMSX-8, especially under thermomechanical fatigue conditions common in jet engines.

Another significant thermal property of turbine blade materials is the coefficient of thermal expansion (CTE). Incompatibility of CTE between the blade material and thermal barrier coatings (TBCs) can result in premature coating delamination. Both CMSX-4 and CMSX-8 exhibit comparatively compatible CTEs with typical TBC systems such as yttria-stabilized zirconia (YSZ) [18], though CMSX-4 Plus has slightly better compatibility, which may increase the life of coated blades.

### Creep and Fatigue Resistance

Creep and fatigue are prevalent failure modes for high-pressure turbine (HPT) blades subjected to high temperatures and cyclic loading. Hence, the evolution of alloys like CMSX-4, CMSX-8, and CMSX-4 Plus has greatly emphasized increasing resistance to these damage mechanisms.

CMSX-4 has been well known for its superior creep resistance at temperatures of up to 1100 °C. This is due to a combination of high-volume fraction of γ′ and optimized solid-solution strengthening by refractory elements such as rhenium (Re) and tungsten (W) [19]. Its creep rupture strength, however, drops considerably when exposed to long-term exposures at temperatures higher than its design limit, which has driven the creation of better variants.

CMSX-8 was developed with higher rhenium content than CMSX-4, and it further raises its creep strength by retarding dislocation mobility and diffusion behavior. High-resolution examinations have determined that CMSX-8 possesses longer creep life at stresses comparable to those encountered in contemporary aero-engine operation [20].

CMSX-4 Plus builds on these developments by adding platinum group metals (PGMs) and minor adjustments to the balance of the alloy. This results in stabilization of the γ/γ′ microstructure on prolonged creep exposure as well as retarding rafting effects that would otherwise reduce the material's strength. Its creep rupture life has been documented at over 1000 hours at 1100 °C and 137 MPa, higher than both CMSX-4 and CMSX-8 under the same conditions [19].

## Method

The approach for analysing the structural integrity of CMSX-4, CMSX-8, and CMSX-4 Plus alloys in HPT blade application was established utilizing finite element analysis (FEA). The analysis consisted of conceptualizing a proper blade geometry, creating a good-quality mesh while considering critical zones, specifying material properties accurately, and imposing boundary conditions that match realistic engine operating environments.

### Geometry

The blade geometry employed in this analysis is a simplified high-pressure turbine blade section. It was optimized to retain the key aerodynamic and structural aspects without unnecessary complexity. The model was a uniform thickness airfoil-shaped profile without internal cooling passages, enabling a straightforward focus on stress and strain behavior under load. Key features like the trailing edge and leading edge were properly preserved to mimic stress concentration regions common in actual turbine blades.

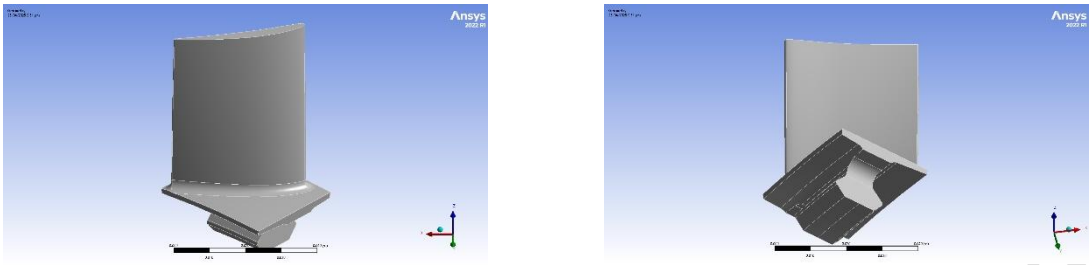

**Figure 1.** Geometry of HPT Blade

## Mesh

A high-quality finite element mesh was created for the blade with tetrahedral elements, with further refinement in areas of importance like the leading edge, trailing edge, and blade root. While a mesh independence study was not specifically reported, the convergence of stress and deformation values in all simulations indicates that the mesh was adequately refined. Higher-order tetrahedral elements were used to capture the curvature and stress gradients in the complex geometry accurately.

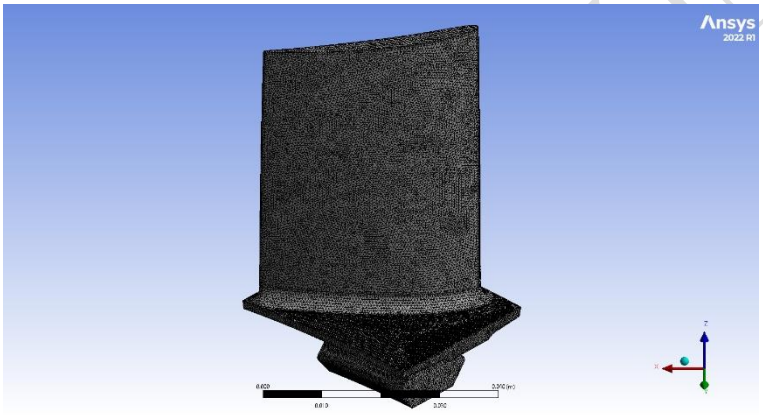

**Figure 2.** Mesh

## Materials

Material properties were defined from experimental data for CMSX-4, CMSX-8, and CMSX-4 Plus. All materials were treated as isotropic and independent of temperature for the scope of this simulation. The most important material properties utilized were density, coefficient of thermal expansion (CTE), Young's modulus, Poisson's ratio, tensile and compressive yield strengths, and ultimate strengths. CMSX-8 showed slightly denser and stronger properties than CMSX-4, whereas CMSX-4 Plus provided intermediate performance between both, with strengthening and thermal stabilization. These properties of the material were essential for the precise forecast of stress and deformation behavior subjected to loads applied.

**Table 1.** Material Properties

| Property | CMSX-4 | CMSX-8 | CMSX-4 Plus |
|---|---|---|---|
| **Density (g/cm³)** | 8.7 | 9.0 | 8.85 |
| **Thermal Expansion Coefficient (CTE)** | $13.5 \times 10^{-6}$ /K | $13.2 \times 10^{-6}$ /K | $13.3 \times 10^{-6}$ /K |
| **Young's Modulus (GPa)** | 210 | 215 | 212 |
| **Poisson's Ratio** | 0.30 | 0.30 | 0.30 |
| **Tensile Yield Strength (MPa)** | 1000 | 1100 | 1050 |
| **Compression Yield Strength (MPa)** | 1000 | 1100 | 1050 |
| **Tensile Ultimate Strength (MPa)** | 1100 | 1200 | 1150 |
| **Compression Ultimate Strength (MPa)** | 1100 | 1200 | 1150 |

### Boundary Conditions

The boundary conditions were judiciously chosen to mimic actual operating conditions. In terms of structure, the root of the blade was completely constrained to mimic being bolted to the turbine disc so that no translation or rotation could occur. Aerodynamic loads were modelled by imposing a uniform pressure load on the blade surface. Thermal boundary conditions were also considered by imposing a constant raised temperature over the blade, typical of usual HPT blade operating conditions, presumed to be approximately 1100°C. These conditions in total provided a realistic simulation of mechanical and thermal stresses encountered during engine operation.

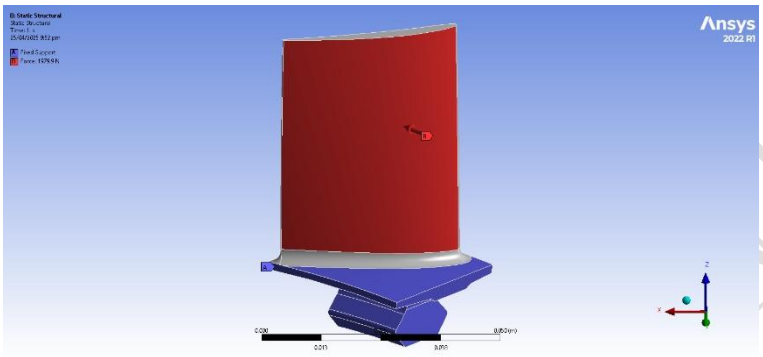


**Figure 3.** Boundary Conditions

## Results and Discussion

The structural behavior of the high-pressure turbine (HPT) blade, which was simulated using three different alloys—CMSX-4, CMSX-8, and CMSX-4 Plus—was examined in depth using finite element analysis (FEA). The analysis concentrated on some of the major output parameters: equivalent von Mises stress, strain, total deformation, and factor of safety (FOS) for each of the alloys. These parameters are essential in determining the material's capacity to meet the stringent operational conditions in turbine engines, with high stresses and temperatures being a norm.

### Stress

The equivalent von Mises stress distribution, which plays a significant role in determining the material failure, was determined to be the same for all three materials under the loading conditions imposed. The highest von Mises stress value achieved throughout the blade for both materials was $8.8796 \times 10^8$ Pa. This consistency in stress distribution is due to the loads and boundary conditions used in the FEA model being constant throughout the analysis. Thus, the only parameter that affected the results was the material properties. Although the von Mises stress was uniform across all materials, it should be noted that stress alone cannot offer a full representation of the material's overall performance. Other determinants like strain, deformation, and the factor of safety give further indications about the structural strength of the blade under working conditions.

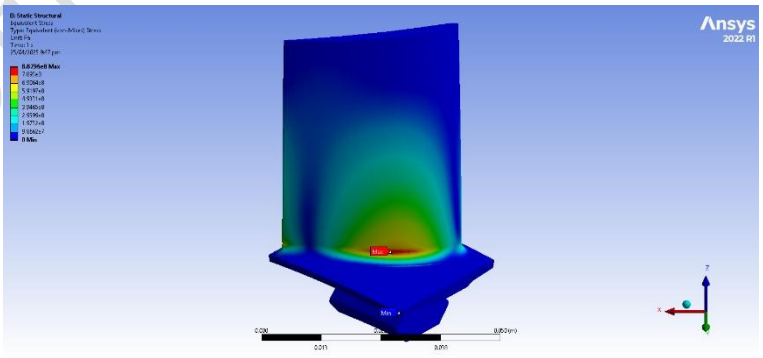


**Figure 4.** Stress Contour of CMSX-4

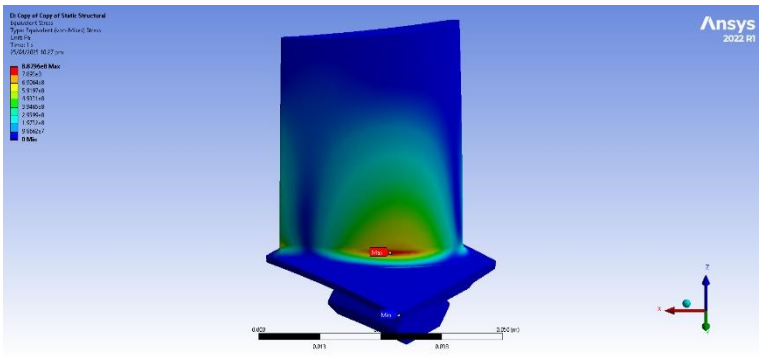


**Figure 5.** Stress Contour of CMSX-8

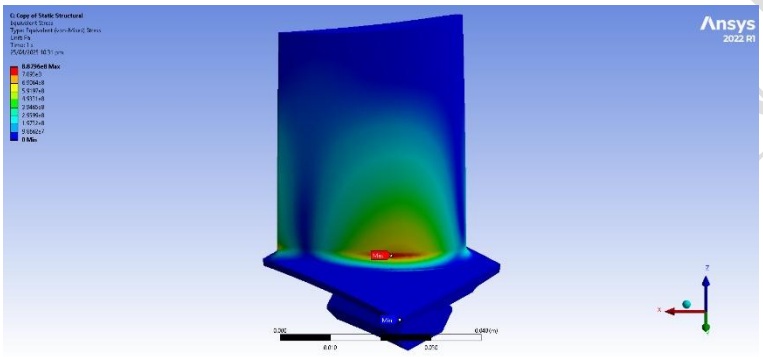


**Figure 6.** Stress Contour of CMSX-4+

**Strain**

The outcomes showed significant variation among the materials. Strain, a measure of relative deformation from the original shape, is a significant parameter to gauge material performance. The material with the largest Young's modulus (a measure of stiffness) was CMSX-8, which registered the lowest value of strain at $4.131 \times 10^{-3}$. This means that CMSX-8 would deform the least elastically under the load applied and therefore is most resistant to deformation among the three. CMSX-4 Plus ranked second with a strain value of $4.1895 \times 10^{-3}$, and CMSX-4 had the largest strain at $4.2294 \times 10^{-3}$. This difference in strain has a direct correlation with the relative stiffness of these materials. The greater the stiffness (Young's modulus), the less deformation will result in a material when stressed. Thus, CMSX-8, being of higher stiffness, deforms the least, and this is a desirable property in high-performance uses like turbine blades.

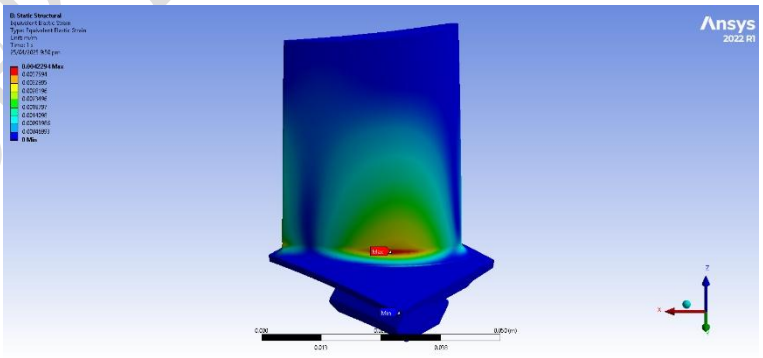


**Figure 7.** Strain Contour of CMSX-4

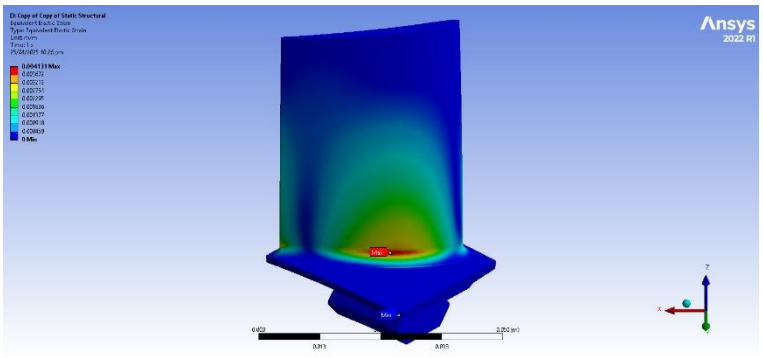


**Figure 8.** Strain Contour of CMSX-8

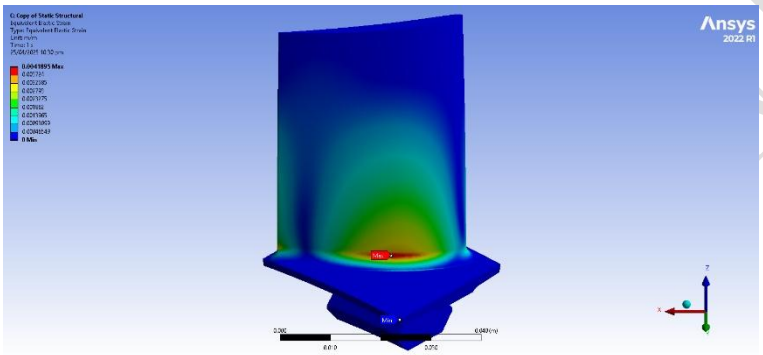


**Figure 9.** Strain Contour of CMSX-4+

**Deformation**

The sum of deformation, which measures the material displacement upon loading, also exhibited the same trend. CMSX-8 registered the smallest value of total deformation at $1.1547 \times 10^{-3}$ m. CMSX-4 Plus, whose stiffness is comparatively high, yielded a slightly increased deformation of $1.171 \times 10^{-3}$ m, and CMSX-4 yielded the highest deformation of $1.1822 \times 10^{-3}$ m. These observations further emphasize the superior stiffness behavior of CMSX-8, which is significant to ensure structural integrity of high-speed rotating turbine blades and thermally stressed blades. The less deformation in CMSX-8 means that it is more effective at maintaining its initial shape during operational stresses, thus lowering the risk of mechanical failure over a period.

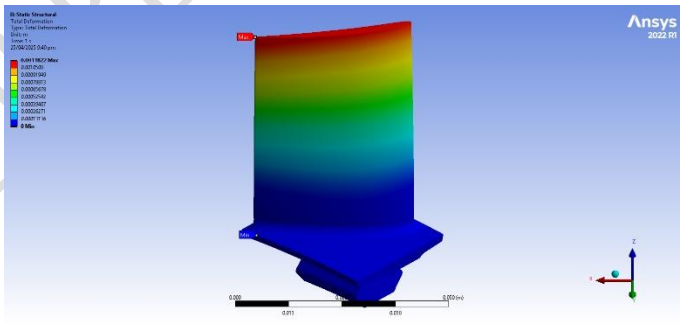


**Figure 10.** Deformation Contour of CMSX-4

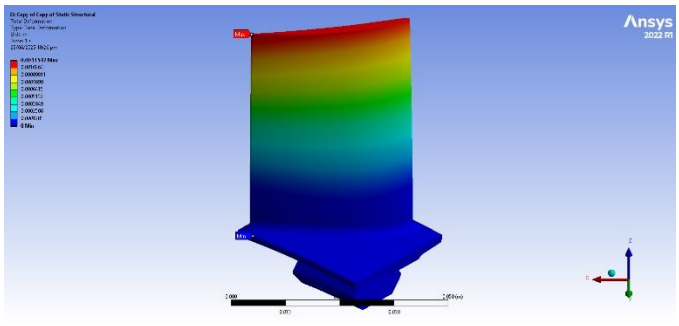


**Figure 11.** Deformation Contour of CMSX-8

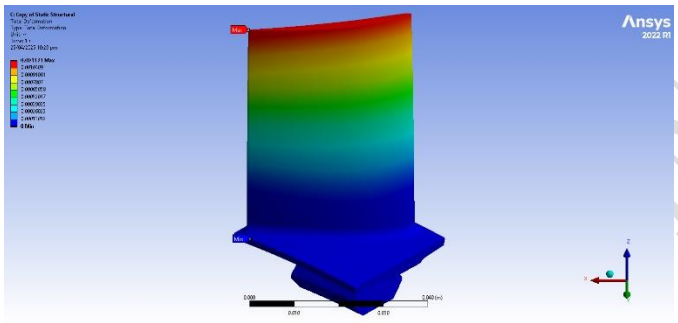


**Figure 12.** Deformation Contour of CMSX-4+

**Factor of Safety**

The FOS is calculated by dividing the material's ultimate strength by the maximum stress experienced by the material under operating conditions. A higher FOS indicates a greater margin of safety, meaning the material is less likely to fail under the applied loads. In this analysis, CMSX-8 achieved the highest FOS of 1.2388, indicating that it has the greatest resistance to failure under the given loading conditions. CMSX-4 Plus came next with an FOS of 1.1825, which is also within the acceptable range, though lower than CMSX-8. CMSX-4, however, had the lowest FOS of 1.1262, indicating that it has a reduced safety margin and is more susceptible to failure than the other two materials under identical conditions. The greater FOS for CMSX-8 indicates its better mechanical properties and capacity to resist higher stresses before failure, thus making it the strongest material for this application.

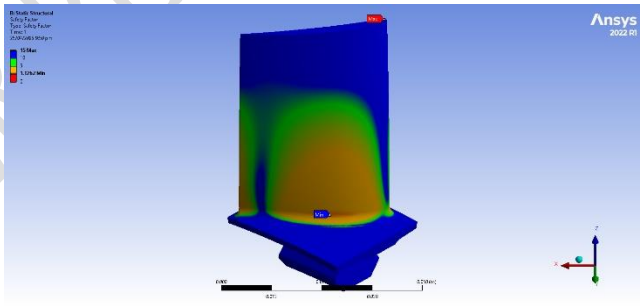


**Figure 13.** FOS Contour of CMSX-4

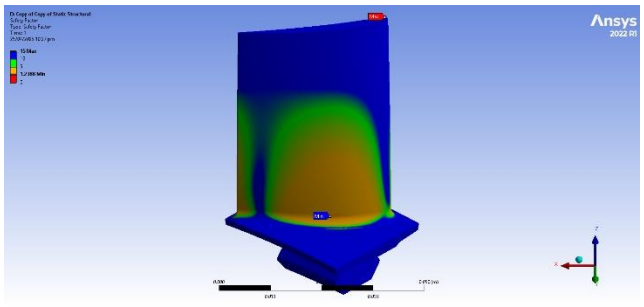


**Figure 14.** FOS Contour of CMSX-8

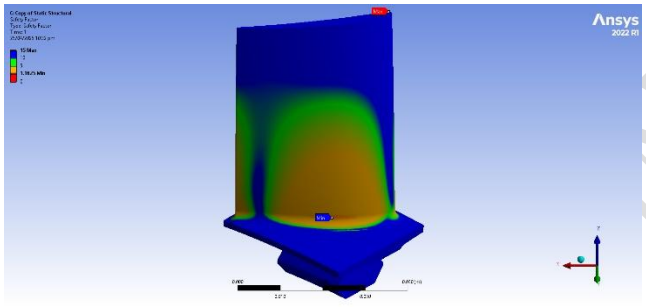


**Figure 15.** FOS Contour of CMSX-4+

Although all three materials—CMSX-4, CMSX-8, and CMSX-4 Plus—are subjected to the same stress levels under the given loads, the variations in their mechanical properties result in very large differences in strain, deformation, and factor of safety. CMSX-8 always proves to be superior to the other two materials as far as resistance to strain, deformation, and factor of safety are concerned, and is thus best suited for such high-performance and reliability-based applications as HPT blades in gas turbines. CMSX-4 Plus provides intermediate performance, with strain resistance and deformation being slightly better than in CMSX-4 but less than that of CMSX-8. These results highlight the significance of material choice in turbine blade design, where a combination of stiffness, strength, and safety is essential to guaranteeing long-term operational reliability. Therefore, CMSX-8 emerges as the most beneficial material for high-performance turbine blades, with greater structural integrity and increased safety margin than CMSX-4 and CMSX-4 Plus.

**Table 2.** Summary of Results

| Property | CMSX-4 | CMSX-8 | CMSX-4 Plus |
|---|---|---|---|
| **Strain** | 4.2294e-003 | 4.131e-003 | 4.1895e-003 |
| **Deformation** | 1.1822e-003 | 1.1547e-003 | 1.171e-003 |
| **Factor of Safety** | 1.1262 | 1.2388 | 1.1825 |
| **Stress** | 8.8796e+008 | 8.8796e+008 | 8.8796e+008 |

## Conclusion

This research effectively tested the structural integrity of a high-pressure turbine (HPT) blade with three state-of-the-art nickel-based single-crystal superalloys, namely CMSX-4, CMSX-8, and CMSX-4 Plus. By performing comprehensive finite element analysis, critical performance indicators such as equivalent stress, strain, deformation, and factor of safety were examined under actual thermal and mechanical loading conditions.

The test results indicated that although all three materials underwent equal stress levels resulting from uniform loading, significant variation was found for strain, deformation, and margins of safety. CMSX-8 had the best overall structure performance with lowest strain and deformation values and maximum factor of safety. This enhanced behavior lies in its designed alloy composition with increased rhenium content to improve creep strength, stiffness, and mechanical toughness. CMSX-4 Plus provided enhanced properties compared to baseline CMSX-4 due to a more perfected microstructure as well as higher thermal stability though still lagging behind CMSX-8 mechanically.

The results serve to emphasize the importance of material selection in optimizing the performance and durability of turbine blades used in high-stress environments. According to the findings of this research, CMSX-8 stands out as the best among the materials investigated, with the greatest balance of strength, stiffness, and safety appropriate for use in high-pressure turbine blades. Follow-on work may follow this up with creep and fatigue simulations under cyclic thermal loading, as well as examination of the performance of these materials with realistic blade geometries such as cooling passages and coatings.

## References


1. D. Dua, M. Khajavi, G. White, D. Thirumurthy, and J. Singh, "Stress Rupture Behavior of Disk Superalloys Exposed to Low-Temperature Hot Corrosion Environment," Proceedings of the ASME Turbo Expo, vol. 10B-2020, Jan. 2021, doi: 10.1115/GT2020-14113.
2. M. Rozmus-Górnikowska, J. Kusiński, Ł. Cieniek, and J. Morgiel, "The Microstructure and Properties of Laser Shock Peened CMSX4 Superalloy," Metall Mater Trans A Phys Metall Mater Sci, vol. 52, no. 7, pp. 2845–2858, Jul. 2021, doi: 10.1007/S11661-021-06277-7/FIGURES/17.
3. N. Chapman, S. Gray, J. Sumner, and J. Nicholls, "Stress Corrosion Testing of CMSX-4, CM247LC DS and IN6203DS Ni-Base Superalloys," Oxidation of Metals, vol. 95, no. 1–2, pp. 85–104, Feb. 2021, doi: 10.1007/S11085-020-10011-W/FIGURES/15.
4. A. Kumar, S. Kumar, and K. N. Pandey, "Life prediction of C3X gas turbine Blade of CMSX-4 material," Advances in Materials and Processing Technologies, vol. 8, no. 4, pp. 4156–4180, Oct. 2022, doi: 10.1080/2374068X.2022.2039425;CTYPE:STRING:JOURNAL.
5. M. Létang, S. Björklund, S. Joshi, D. Sebold, O. Guillon, and R. Vaßen, "Repair of Single-Crystal CMSX-4 Using the High Velocity Air Fuel Process," Journal of Thermal Spray Technology, pp. 1–18, Feb. 2025, doi: 10.1007/S11666-025-01944-2/FIGURES/19.
6. K. Durst and M. Göken, "Micromechanical characterisation of the influence of rhenium on the mechanical properties in nickel-base superalloys," Materials Science and Engineering: A, vol. 387–389, no. 1-2 SPEC. ISS., pp. 312–316, Dec. 2004, doi: 10.1016/J.MSEA.2004.03.079.
7. B. G. Choi, C. Y. Jo, H. U. Hong, I. S. Kim, S. M. Seo, and H. M. Kim, "Effect of pre-strain on microstructural evolution during thermal exposure of single crystal superalloy CMSX-4," Transactions of Nonferrous Metals Society of China (English Edition), vol. 21, no. 6, pp. 1291–1296, Jun. 2011, doi: 10.1016/S1003-6326(11)60855-8.
8. W. Xia et al., "New strategy to improve the overall performance of single-crystal superalloys by designing a bimodal γ′ precipitation microstructure," Acta Mater, vol. 257, p. 119200, Sep. 2023, doi: 10.1016/J.ACTAMAT.2023.119200.
9. Z. Shang et al., "Microstructure and mechanical properties of a new nickel-based single crystal superalloy," Journal of Materials Research and Technology, vol. 9, no. 5, pp. 11641–11649, Sep. 2020, doi: 10.1016/J.JMRT.2020.08.032.
10. Y. Song et al., "New insights into the optimisation of the solution heat treatment process and properties of CMSX-4 superalloys," Materials Science and Engineering: A, vol. 890, p. 145947, Jan. 2024, doi: 10.1016/J.MSEA.2023.145947.
11. Y. Cheng, X. Zhao, W. Xia, Q. Yue, Y. Gu, and Z. Zhang, "The overview of the formation mechanisms of topologically close-packed phases in Ni-based single crystal superalloys," Mater Des, vol. 237, p. 112582, Jan. 2024, doi: 10.1016/J.MATDES.2023.112582.
12. T. Wang et al., "Effect of temperature on tensile behavior, fracture morphology and deformation mechanisms of Nickel-based single crystal CMSX-4," J Alloys Compd, vol. 912, p. 165175, Aug. 2022, doi: 10.1016/J.JALLCOM.2022.165175.
13. Y. M. Li et al., "Carbon addition and temperature dependent tensile deformation resistance and capacity of a low-cost 3rd-generation Ni-based single crystal superalloy," Mater Charact, vol. 210, p. 113794, Apr. 2024, doi: 10.1016/J.MATCHAR.2024.113794.

14. N. Wijeyeratne, F. Irmak, N. O'nora, and A. P. Gordon, "A Comparative Study of Constitutive Modeling of an Aero-Engine Single Crystal Superalloy under Creep-Thermomechanical Fatigue," AIAA Science and Technology Forum and Exposition, AIAA SciTech Forum 2022, 2022, doi: 10.2514/6.2022-0629.
15. K. Harris and S. Cannon, "CMSX-4® Plus Single Crystal Alloy Development, Characterization and Application Development: Proceedings of the 13th Intenational Symposium of Superalloys," 2016, doi: 10.1002/9781119075646.ch3.
16. D. Li et al., "High temperature oxidation behavior of Ni-based superalloy Nimonic95 and the effect of pre-oxidation treatment," Vacuum, vol. 194, p. 110582, Dec. 2021, doi: 10.1016/J.VACUUM.2021.110582.
17. D. Tarasov, A. Tyagunov, and O. Milder, "Simulation of the nickel superalloys solvus temperature by the deep learning artificial neural network with differential layer," AIP Conf Proc, vol. 2611, no. 1, Nov. 2022, doi: 10.1063/5.0119488/2830385.
18. R. T. Wu and R. C. Reed, "On the compatibility of single crystal superalloys with a thermal barrier coating system," Acta Mater, vol. 56, no. 3, pp. 313–323, Feb. 2008, doi: 10.1016/J.ACTAMAT.2007.07.057.
19. D. Li et al., "Long-term aging behavior and mechanism of CMSX-4 nickel-based single crystal superalloy at 950 ℃ and 1050 ℃," J Alloys Compd, vol. 1004, p. 175763, Nov. 2024, doi: 10.1016/J.JALLCOM.2024.175763.
20. E. A. Estrada Rodas, S. Gorgannejad, and R. W. Neu, "Creep-fatigue behaviour of single-crystal Ni-base superalloy CMSX-8," Fatigue Fract Eng Mater Struct, vol. 42, no. 9, pp. 2155–2171, Sep. 2019, doi: 10.1111/FFE.13098.